Adhesion-Related Failure Mechanisms in Micromechanical Devices

C. H. Mastrangelo

Abstract— **Adhesion-related failures occurs in microelectromechanical systems (MEMS) when suspended elastic members unexpectedly stick to their substrates. This type of device failure is one of the dominant sources of yield loss in MEMS. This paper reviews the physical mechanisms responsible for the failure from both the theoretical and practical stand point. In general, the failure requires two different phenomena. First (a) the device must be subject to a force sufficiently strong to collapse the elastic member thus bringing it in contact with the substrate. (b) After contact is established and the force removed, the intersolid adhesion must exceed the elastic member restoring force hence keeping the device permanently pinned to the substrate. Both of these problems develop during the device fabrication as well as during the device operation. Normalized elastic member dimension bounds for prevention of collapse and pinning are presented. The failure rate can also be reduced using a wide variety of processing, surface treatment, and physical schemes. These are discussed in regard to their practical applicability.**

Keywords— **Adhesion in MEMS**

I. Introduction

Microlectromechanical systems are micrometer-size systems capable of interfacing electrical world to mechanical signals. These devices have a wide variety of applications performing basic signal transduction operations as sensors and actuators. MEMS are usually constructed using lithographic processes derived from VLSI technology.

Because these devices must react to mechanical signals, many of these use construction topologies that require physical motion. For example, an accelerometer-type device translates the motion of a suspended proof mass into capacitance which is later converted to a voltage output. Similarly, micromechanical mirrors must be able to deflect a light beam in a particular direction. Suspended micromachined structures such as plates and beams are commonly used in the manufacturing of pressure [1–4] and acceleration sensors [5, 6]. These structures are typically made by forming a layer of the plate or beam material on top of a sacrificial layer of another material and etching the sacrificial layer [7, 3].

These microstructures have relatively large areas, but a very small stiffness. At the same time these elements are fabricated a few microns from their supporting substrate. The combination of these three characteristics makes MEMS devices highly susceptible to surface forces which can cause the suspended members to deflect toward the substrate. Under certain conditions, the elastic member can collapse and permanently adhere to their underlying substrates causing a device failure. Namely, this can happen both during the device fabrication and normal use.

During processing, adhesion can occur when the suspended member is exposed to an aqueous rinse and dry cycle. Since the device-to-substrate gap is so small, strong attractive capillary forces can develop during the dehydration causing its collapse and subsequent pinning to the substrate. [7–11]. Nathanson and Guldberg [12] recognized that small mechanical structures are influenced by surface tension forces. Guckel and Burns [7] observed that when microscopic elastic plates are rinsed and dried, the capillary forces acting on these are large enough to bring them in contact with their underlying substrate. They also observed that, after complete drying, some of them remain pinned to the substrate held by attractive forces rendering them unusable. A number of researchers have proposed different mechanisms to explain these forces. Scheeper *et al.* [9] proposed that the adhesion is caused by water molecules adsorbed on the adhering surfaces [13]. Alley *et al.* [14] proposed that the adhesive bond is formed by silica residues that remain on the substrate after the water has evaporated.

The same collapse can develop when the device is under normal operation if it is exposed to high humidity conditions leading to capillary condensation [15] (hence the formation of a water droplet in the gap). A third yet possible adhesion failure mode develops if the suspended member is placed in contact with its substrate by external forces. This may be done by the deliberate placement of a collapsing force or by accidental shock.

The pinning process is hence divided into two stages of (a) mechanical collapse and (b) adhesion to the substrate. If any two of these is eliminated, the adhesion failure does not occur. In practice, either mechanism can be prevented provided the stiffness of the microstructure is high enough. Therefore there exists a characteristic physical parameter that determines the onset of the failure. The presence of the failure threshold is readily observed experimentally by constructing an array of progressively weaker suspended elements followed by examination of the sticking condition. Figure 1 shows a photograph of an array of micromachined polysilicon cantilever beams showing clearly the onset of the pinning condition at a particular beam *detachment length*. The same phenomena happens for other suspended micromachined structures such as doubly supported beams and plates as shown in Figure 2.

This paper discusses a general review of the causes for these phenomena and several common techniques used to alleviate the problem. In Sections II and III we discuss theoretical models for both stages, and provide two bounds on the physical dimensions of the suspended member that eliminate the failure. In Sections IV and V various techniques used to eliminate the adhesion failure are discussed. These are divided onto physical schemes that attempt to minimize the contact area and chemical schemes that minimize the intersolid adhesion. The paper concludes with some general comments about the practicality of the methods at hand.

Department of Electrical Engineering and Computer Science, University of Michigan, Ann Arbor, MI 48109-2122, USA

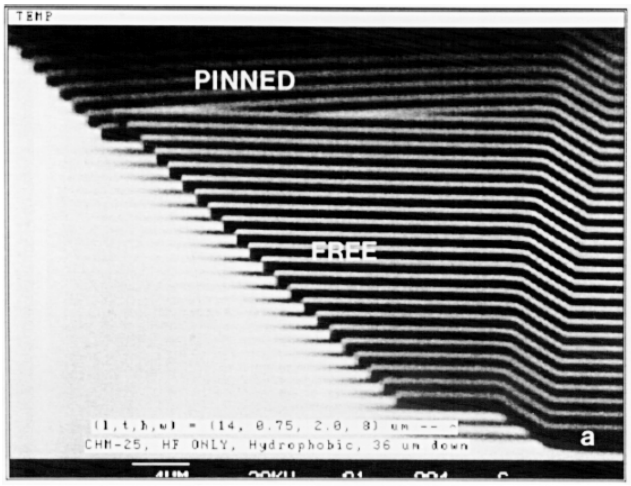

Fig. 1. SEM of micromachined polysilicon cantilever beams of increasing length. The photograph shows clearly the onset of the pinning state for beams larger than 34 μm.

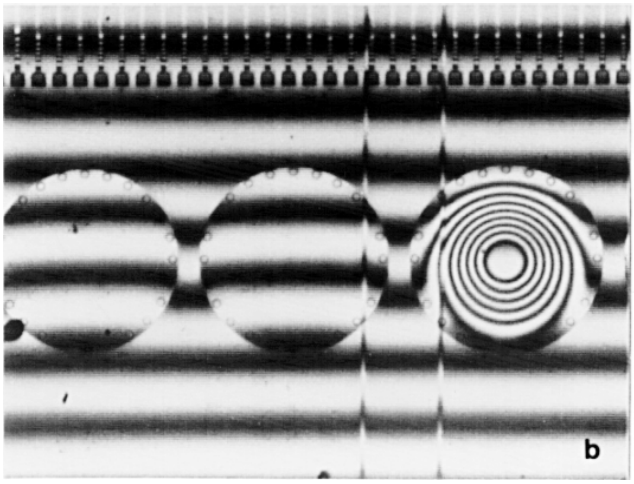

Fig. 2. Interferometric microphotograph of an array of micromachined polysilicon circular plates. The structures with circular interference patterns are pinned to the substrate.

II. Mechanical Collapse by Capillary Force

Suspended elements in MEMS are typically fabricated by first forming a layer of the plate or beam material on top of a sacrificial layer of another material and etching the sacrificial layer [7, 3]. If the etch is performed in a liquid environment, as the liquid is removed during a dehydration cycle, a liquid bridge is formed between the suspended member and the substrate yielding an attractive capillary force which may be sufficiently strong to collapse it. The capillary force is essentially determined by the change in the wetting area of the liquid bridge. The elastic force is linearly proportional to the deflection. The unifying quantity is the liquid bridge volume which at a given time remains constant.

The behavior of elastic structures under capillary forces has been studied in [16]. Here, as an illustrative example, we analyze the simplified lumped elastic structure of Figure 3 in which the plate represents the suspended member surface, the spring its stiffness, and the gap the distance between the member and the substrate. This simplified structure proves useful in understanding the mechanical stability of the suspended member as well as the general behavior of elastic microstructures under a capillary pull. In Figure 3, a rigid circular plate of radius r_o is suspended

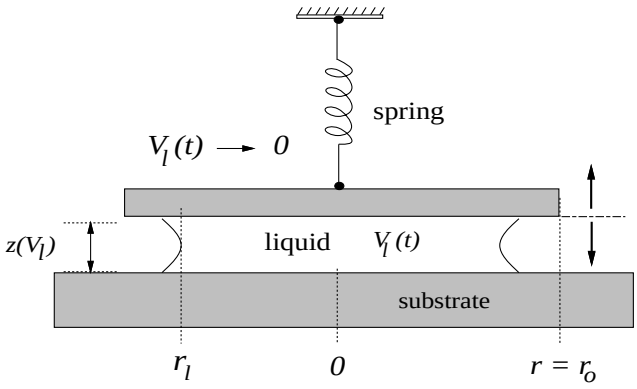

Fig. 3. Deflection of a rigid plate attached to a spring by capillary forces

above a substrate. The substrate is fixed, and the top plate is attached to a spring of constant κ. If the weight of the plate is negligible, the original plate separation is $z = h$ when the spring is relaxed. A liquid bridge of volume V_l is trapped between the plate and substrate. In order to simulate the drying process, the equilibrium positions assumed by the plate as the liquid is gradually removed are considered. Initially, the liquid spreads to a radius r_l with a volume $V_l = \pi r_l^2 z$. The maximum volume that the liquid assumes without overflowing is $V_o = \pi r_o^2 h$. The surface energy U_S of the spring-plate-liquid system is

$$U_S = \begin{cases} U_{S_o} + 2\pi\gamma_l \cos\theta_c \left(r_o^2 - V_l/\pi z \right) & z \geq z^* \\ U_{S_o} + \pi\gamma_l (\cos\theta_c - 1) \left(r_o^2 - V_l/\pi z \right) & z < z^* \end{cases} , \tag{1}$$

where U_{S_o} is a constant, θ_c is the contact angle, γ_l is the liquid surface tension, and $z^* = V_l/\pi r_o^2$ is the plate separation assumed when the liquid completely wets the surface of the top plate. This equation neglects the complicated nature of the small liquid-air meniscus area [17–21] since the liquid-air area is small, or $2\pi r_l z << 2\pi r_l^2$. At $z = z^*$, U_S has a breakpoint, and for $z < z^*$, the liquid overflows. Initially, the total energy is

$$\begin{aligned} U_T &= U_S + U_E \\ &= U_{S_o} + 2\pi\gamma_l \cos\theta_c \left(r_o^2 - \frac{V_l}{\pi z} \right) + \frac{1}{2}\kappa (h - z)^2 \end{aligned} \tag{2}$$

The equilibrium plate spacing minimizes U_T. Figure 4 shows plots of U_T for different liquid volumes. The curve has one or two minima. One of these develops at the breakpoint of U_S implying that the equilibrium liquid radius is r_o. The other results when $dU_T/dz = 0$ or from Eq. (2) along the curve

$$z^2(z - h) - \frac{2\gamma_l \cos\theta_c \, V_l}{\kappa} = 0 . \tag{3}$$

The path traced by the reachable minimum of U_T as the liquid volume decreases from $V_l = V_o$ to $V_l = 0$ determines the equilibrium position and final state of the plate. This path is known as the equilibrium trajectory, and a reachable minimum of a potential system is that at which the system rests from a known starting state. Conceptually, this minimum is determined by placing

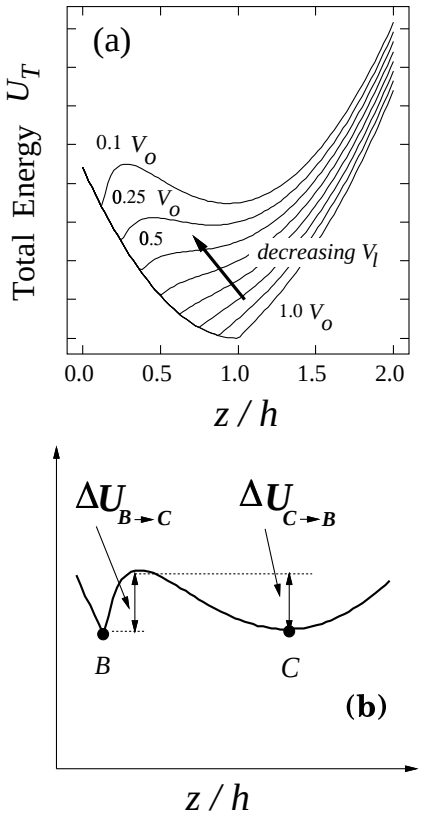

Fig. 4. (a) Total energy of the two-plate system. (b) Activation energy separating the minima

an imaginary golf ball on the energy curve at any starting position and letting it roll to the most favorable energy well. As internal control parameters change, the shape of the curve and its minima shift making the ball slide toward one side or the other (see Figure 5). Sudden changes or *catastrophes* may occur in the equilibrium for those values of the parameters at which a local minimum disappears when it merges with a local maximum [22–25].

The behavior of the spring-plate-liquid system during the drying cycle is evident when the branches of the local extrema of U_T are plotted as a function of the control parameter V_l in a branching diagram. Letting $\xi = V_l/V_o$, $\lambda = z/h$ and $V_o = \pi r_o^2 h$, the first branch $\mathcal{B}_\infty$ associated with an extremum in U_S is

$$\mathcal{B}_\infty : \; V_l \; = \; \pi r_o^2 z \; , \text{ or } \; \xi = \lambda \; . \tag{4}$$

The second branch $\mathcal{B}_\in$ is found from Eq. (3)

$$\mathcal{B}_\in : \; \xi = \left(\frac{\kappa\, h^2}{2\pi\gamma_l \cos\theta_c \; r_o^2}\right)(1-\lambda)\lambda^2 \; = \; N_C \; (1-\lambda)\lambda^2 \; , \tag{5}$$

where the non-dimensional number $N_C = \kappa\, h^2/2\pi\gamma_l \cos\theta_c \; r_o^2$. Branch $\mathcal{B}_\in$ is a minimum of U_T for $\lambda > 2/3$ and a maximum for $\lambda < 2/3$. Figure 6 shows three branching diagrams for fixed N_C. The arrows show the direction of the equilibrium trajectories.

In Figure 6(a), the equilibrium trajectory begins at A with $(\xi, \lambda) = (1, 1)$. If N_C is low, branches $\mathcal{B}_\infty$ and $\mathcal{B}_\in$ do not intersect. As V_l decreases, the trajectory follows branch $\mathcal{B}_\infty$ from

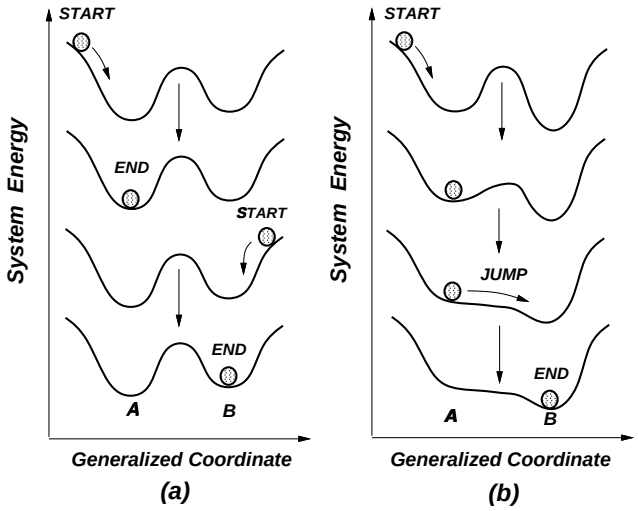

Fig. 5. (a) Reachable minima of a potential system. (b) Catastrophe.

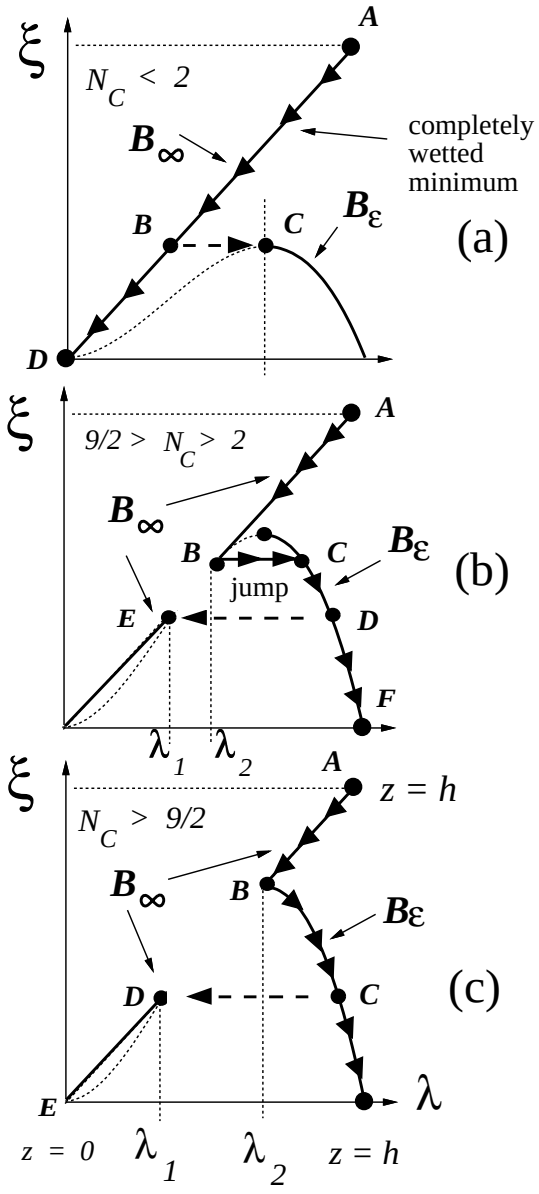

Fig. 6. Branching diagrams for the spring-plate-liquid system

points A to B. At $\xi(B)$ a second minimum C from $\mathcal{B}_\in$ emerges in the energy curve. This new minimum is not reachable since an energy barrier $\Delta U_{B\to C}$ is present between the two minima as shown in Figure 4(b). In the limit as $V_l \to 0$, the trajectory ends at D with $(\xi,\lambda) = (0,0)$. The final plate separation is $z = 0$, and the plate remains pinned to the substrate.

N_C can be adjusted such that $\mathcal{B}_\infty$ and $\mathcal{B}_\in$ intersect in a segment as in Figure 6(b). Setting $\mathcal{B}_\infty(\lambda) = \mathcal{B}_\in(\lambda)$ one finds

$$\xi \;=\; (\lambda_1,\lambda_2) \;=\; \frac{1}{2} \pm \left(\frac{1}{4} - \frac{1}{N_C}\right)^{1/2} . \qquad (6)$$

When λ_1 and λ_2 are real, the segments of $\mathcal{B}_\infty$ and $\mathcal{B}_\in$ in $\lambda_1 \le \lambda \le \lambda_2$ combine thus disappearing from the extremum set. The equilibrium trajectory starts at A following branch $\mathcal{B}_\infty$ to B. At $\xi(B)$, the trajectory jumps abruptly to the now global minimum at point C and continues along $\mathcal{B}_\in$ to point D where the minimum E from $\mathcal{B}_\in$ reappears. Point E is is not reachable because of the barrier $\Delta U_{D\to E}$; thus, for lower V_l, the trajectory follows $\mathcal{B}_\in$ ending at F with $(\xi,\lambda) = (0,1)$. The final plate separation is $z = h$, and the plate is free.

There is a threshold value in N_C, defined as N_T, that determines the final state. Trajectories with $N_C < 4$ follow $\mathcal{B}_\infty$ throughout the cycle, yielding pinned plates. Trajectories with N_C slightly larger than 4 are routed to branch $\mathcal{B}_\in$ after a catastrophe yielding free plates. For $N_C \ge 9/2$ and $\lambda_2 \ge 2/3$, the trajectory is a smooth curve (Figure 6(c)) yielding free plates; thus $N_T = 4$.

It is convenient to define an *elastocapillary number*, N_{EC}, such that the plate is free for $N_{EC} > 1$ and pinned for $N_{EC} < 1$. Thus

$$N_{EC} \;=\; \frac{N_C}{N_T} \;=\; \left(\frac{\kappa\, h^2}{8\pi\, \gamma_l \cos\theta_c\, r_o^2}\right) . \qquad (7)$$

In practice, the free/pinned transition defined by N_{EC} is not sharp. If the plates acquire sufficient kinetic energy through agitation to overcome the energy barriers, the plate has a nonzero probability of transition between the various equilibrium states; thus a few plates may be free when $N_{EC} < 1$ and others may be pinned when $N_{EC} > 1$.

The analysis of the simple spring-plate-liquid system shows (a) a bifurcation of the equilibrium trajectory, and (b) a non dimensional parameter which determines its final free/pinned state. These characteristics are also present in continuous elastic structures. In [16], expressions for the elastocapillary numbers for continuous elastic beams and plates have been calculated using a variational energy approach that includes the elastic, potential, and surface energies. The results for different microstructures are shown in Table I. where E is the Young modulus, t the member thickness, h the gap, ν is Poisson's ratio, σ_R the member residual tensile stress, and l, w, r_o are the member length, width, and radius.

III. Pinning by Contact Adhesion

The second phenomena required to produce the failure is an intersolid adhesion that can overcome the restoring force of the elastic member. The adhesion force is a consequence of the change in the energy stored at the contact area with respect to the member deformation. In real surfaces, the magnitude of the adhesion energy is highly dependent on the nature of the interface. Typically, in strong crystalline solids this energy is very high (500-2000 mJm^{-2}), and in soft solids, such as polymers, it is very low (5-100 mJm^{-2}).

In this section we consider the equilibrium between these two opposing forces using an energy function formulation that includes the adhesion and elastic energy of the deformed member and determine physical bounds on the elastic member dimensions sufficient for the prevention of failure.

As an illustrative example, consider the peeling of an elastic cantilever beam from an adhesive surface. This problem is related to the peeling of sticky tapes [26] and the cleavage of crystals [27–29]. Figure 7 shows a cross section of a cantilever

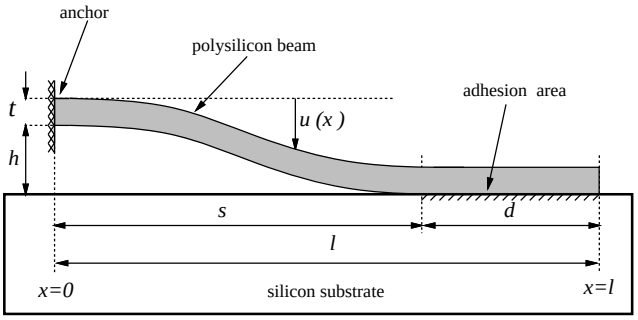

Fig. 7. Schematic of cantilever beam adhering to the substrate

beam of length l, width w, thickness t, height h, and Young's modulus E. The beam is adhering to its substrate a distance $d = (l - s)$ from its tip. The stored elastic energy of the beam in the segment $0 \le x \le s$ induces a restoring force that tends to peel the beam from the adhering substrate. The energy of adhesion stored in the segment $s \le x \le l$ induces another force that holds the beam in contact with the substrate. The equilibrium peel distance s^* is determined by the balance of these two energies. At equilibrium, s^* minimizes the the total energy of the system (bending plus adhesion energies) [26].

Since there are no external forces acting on the beam for $0 \le x \le s$, its deflection $u(x)$ is the solution of

$$E\,I\,\frac{d^4u}{dx^4} \;=\; 0 \quad , \quad I \;=\; \frac{wt^3}{12} \;, \qquad (8)$$

where I is the moment of inertia of the beam respect to the z axis. Equation (8) is solved subject to the boundary conditions

$$\left.\frac{du}{dx}\right|_0 \;=\; \left.\frac{du}{dx}\right|_s \;=\; 0 \;, \quad u(0) \;=\; 0 \;, \quad u(s) \;=\; h \;. \qquad (9)$$

which ignores the effects of finite compliance at the step-up posts [30, 31].
Equation (8) has the solution

$$u \;=\; h\,f(\eta) \;=\; h\eta^2(\,3 - 2\eta\,) \quad , \quad \eta \;=\; \frac{x}{s} \;. \qquad (10)$$

The bending energy stored in the beam is

$$U_E \;=\; \frac{EI}{2}\int_0^l \left(\frac{d^2u}{dx^2}\right)^2 dx \;=\; \frac{6EIh^2}{s^3} \;. \qquad (11)$$

TABLE I

APPROXIMATE ELASTOCAPILLARY NUMBERS FOR DIFFERENT MICROSTRUCTURES

Structure	*Approximate Elastocapillary Numbers*
cantilever beam	$\dfrac{2Eh^2t^3}{9\gamma_l\cos\theta_c l^4(1+t/w)}$
doubly supported beam	$\dfrac{128Eh^2t^3}{15\gamma_l\cos\theta_c l^4(1+t/w)}\left[1+\dfrac{2\sigma_R l^2}{7Et^2}+\dfrac{108h^2}{245t^2}\right]$
circular plate	$\dfrac{10}{9}(\dfrac{5}{2})^{2/3}(\dfrac{Eh^2t^3}{\gamma_l\cos\theta_c(1-\nu^2)r_o^4})\left[1+\dfrac{3(1-\nu^2)}{4}\dfrac{\sigma_R r_o^2}{Et^2}+\dfrac{2187}{2560}(\dfrac{2}{5})^{2/3}(\dfrac{h^2}{t^2})\right]$
square plate	$(\dfrac{25Eh^2t^3}{\gamma_l\cos\theta_c(1-\nu^2)w^4})\left[1+\dfrac{2(1-\nu^2)}{9}\dfrac{\sigma_R w^2}{Et^2}+\dfrac{5}{12}\dfrac{h^2}{t^2}\right]$

The interfacial adhesion energy stored in $s \le x \le l$ is simply the surface energy per unit area of the bond γ_s times the area of contact

$$U_S = -\gamma_s w(l-s) \ . \tag{12}$$

The parameter γ_s has units of $\mathrm{J\,m^{-2}}$ or $\mathrm{N\,m^{-1}}$. The sign of U_S is negative because it is a binding energy. The total energy (or free energy) of the system is the sum of the elastic plus surface energies

$$U_T = U_E + U_S = \frac{6EIh^2}{s^3} - \gamma_s w(l-s) \ . \tag{13}$$

Figure 8 shows a typical curve of $U_T(s)$. This curve has a single minimum corresponding to the equilibrium s^*. This is found by

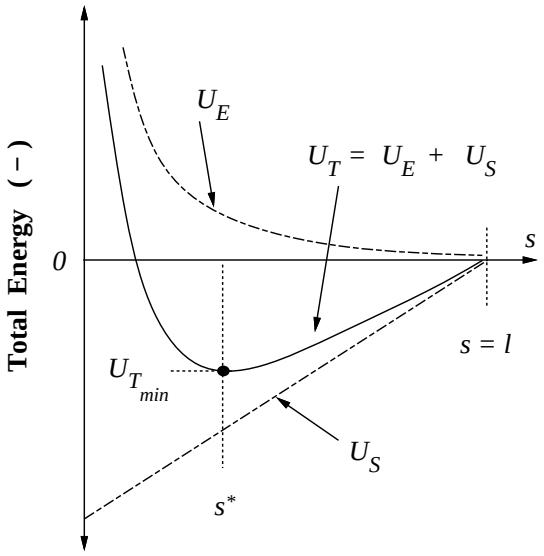

Fig. 8. Typical total energy curve for cantilever beam adhering to the substrate.

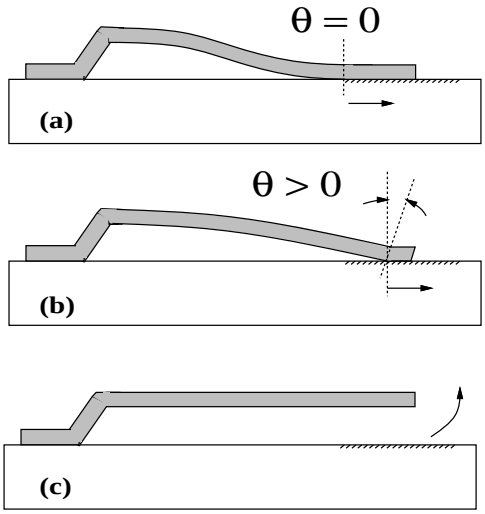

Fig. 9. Pivoting of cantilever tip near detachment.

setting $dU_T/ds = 0$ to obtain

$$s^* = \left(\frac{3}{2}\frac{Et^3h^2}{\gamma_s}\right)^{1/4} \ . \tag{14}$$

The energy curve has a single equilibrium point if $s^* < l$ and no equilibrium point if $s^* > l$. Thus the beam is pinned to the substrate if $s^* < l$, and it is free if $s^* > l$.

The slope boundary condition $du/dx = 0$ at $x = s$ does not allow for shear deformations of the tip of the beam. Shear deformations are particularly important for $s \to l$ since when $d = (l-s)$ is very small, the tip of the cantilever "pivots" changing its elastic energy substantially just before detachment as shown in Figure 9. This effect is taken into consideration by dividing the beam into two regions. The region of the beam for

$0 < x < s$ has no external forces acting on it, so Eq. (8) is solved subject to the boundary conditions of Eq. (9) and the modified slope condition at $x = s$,

$$\left.\frac{du}{dx}\right|_s = \theta = \frac{hm}{s} \quad . \tag{15}$$

where θ is the shear angle of the tip, and m is a non dimensional number. The deflection $u(x)$ and elastic energy of the beam segment are

$$u = h\eta^2((m-2)\eta + (3-m)) \quad , \tag{16}$$

$$U_E = \frac{6EIh^2}{s^3}\left(1 - m + \frac{1}{3}m^2\right) \quad .$$

Note that U_E decreases with increasing m (and θ) for $0 \le m \le 3/2$. The short segment $s \le x \le l$ corresponding to the beam tip experiences shear deformations which determine m. The solution of the coupled problem is given in reference [32] yielding

$$m(s) = \frac{\frac{16}{5}\left(\frac{t}{d}\right)^3\left(\frac{t}{s}\right)\left[1 + \frac{15}{32}\left(\frac{d}{t}\right)^2\frac{E}{G}\right]}{1 + \frac{32}{15}\left(\frac{t}{d}\right)^3\left(\frac{t}{s}\right)\left[1 + \frac{15}{32}\left(\frac{d}{t}\right)^2\frac{E}{G}\right]} \tag{17}$$

where $G = E/2(1+\nu)$ is the beam shear modulus.

The beam detaches from its substrate when

$$l = s^* = \left(\frac{3}{8}\frac{Et^3h^2}{\gamma_s}\right)^{1/4} \tag{18}$$

therefore we can define a *peeling bound*, N_P such that the beam remains in contact with the substrate for $N_P < 1$ and free for $N_P > 1$. Thus

$$N_P = \frac{3}{8}\frac{Et^3h^2}{\gamma_s l^4} \tag{19}$$

Using the same techniques, peel bounds for doubly-supported beams and plates have been calculated. These bounds are shown in Table II.

Figures 10-12 shows experimental plots of the effectiveness of some of the bounds for different structures. The best fit occurs for cantilever beams because of the lack of residual and elongation stresses. The surface energies have been determined from the slope of the plot. Surface energies ranging between 100-300 mJm^{-2} have been measured for polysilicon microstructures [16].

While these bounds are useful for detecting the onset of adhesion-related failures in MEMS devices, many practical devices require dimensions that fall within the failure range. This is one of the motivations for developing thicker structures (with higher h and t) using LIGA-type processes [33, 34].

A number of schemes have been developed to alleviate the pinning failure both during the fabrication and device operation. These schemes are directed toward both the elimination the collapsing force and the reduction of the intersolid adhesion. Roughly, these schemes fall within two categories. Physical schemes aim to modify the shape of the structure to minimize these forces forces. Chemical schemes aim toward the chemical modification of the contact surfaces through the use of low-energy coatings. These are discussed in the sections below.

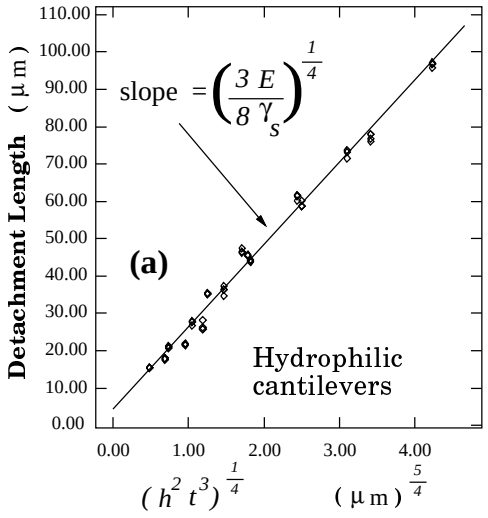

Fig. 10. Peel bound for polysilicon cantilever beams

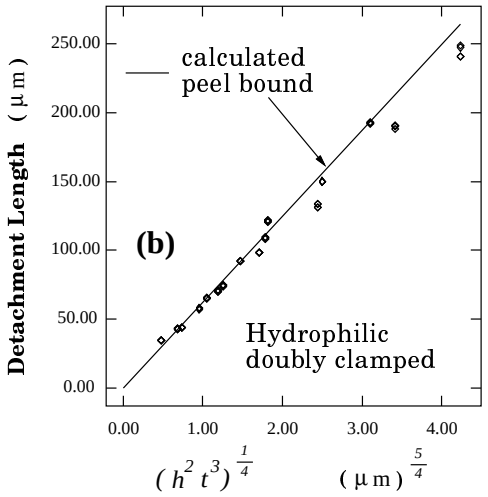

Fig. 11. Peel bound for doubly supported beams

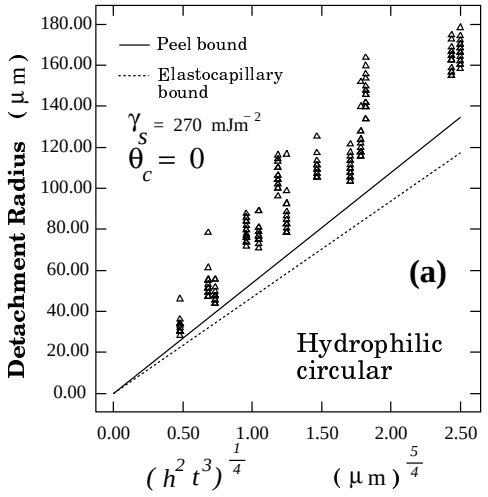

Fig. 12. Peel bound for polysilicon circular plates

TABLE II
APPROXIMATE PEEL NUMBERS FOR DIFFERENT MICROSTRUCTURES

Structure	*Approximate Peel Numbers*
cantilever beam	$\frac{3}{8}\frac{E t^3 h^2}{\gamma_s l^4}$
doubly supported beam	$\left(\frac{128 E h^2 t^3}{5\gamma_s l^4}\right)\left[1+\frac{4\sigma_R l^2}{21 E t^2}+\frac{256}{2205}(\frac{h}{t})^2\right]$
circular plate	$\frac{40}{3}\frac{E h^2 t^3}{(1-\nu^2)\gamma_s r_o^4}\left[1+\frac{51(1-\nu^2)}{160}\frac{\sigma_R r_o^2}{E t^2}+\frac{63}{200}\frac{h^2}{t^2}\right]$
square plate	$\frac{186 E h^2 t^3}{(1-\nu^2)\gamma_s w^4}\left[1+\frac{27(1-\nu^2)}{310}\frac{\sigma_R w^2}{E t^2}+\frac{12}{31}\frac{h^2}{t^2}\right]$

IV. ELIMINATION OF COLLAPSING FORCE

A large number of adhesion failures occur during the fabrication of the devices themselves. These failures are related to the capillary force that develops when the structures are released by wet chemical etches. The capillary pull force can be eliminated if the liquid phase is not present. Several techniques have been based upon this idea.

It is worth noting that biologists [35] have struggled through the same problems much earlier. It is well known that capillary forces are responsible for the collapse of fragile microscopic biological specimens. Many methods have been developed to solve this problem. Almost all of these methods have been rediscovered and applied to MEMS structures with various degrees of success.

A. Freeze-Drying Methods:

The rinse solution can be removed by freezing the solution and sublimation. This freeze-drying [36–38] technique can be used to eliminate the capillary pull by freezing the sample and then exposing it to a heated vacuum environment. This was first applied to the release of MEMS devices by Guckel and Burns [7]. A well known disadvantage of the freeze-drying method is the fact that the rinse solution can undergo a significant volume change. This volume change can create a stress sufficient to destroy the sample. The above authors used a cryoprotectant rinse solution consisting of a mixture of methanol and water that minimized the volume change. A similar process was developed by Takeshima *et al.* [11] by replacing the rinse solution through a gradual series of dilutions with t-butyl alcohol which freezes at 25.6 C°. The freeze-drying technique is now rarely used and has been replaced by the more successful supercritical drying technique described below.

B. Supercritical Drying:

Another method of eliminating the capillary pull is by the use of supercritical drying techniques. In this technique, the rinse solution is gradually replaced by liquid CO_2 at elevated pressures inside a high-pressure chamber. The sample is then taken to the critical point of CO_2 where the interface between the liquid and gas does not exists. The technique is highly successful with nearly 100% yields [39]. Commercial supercritical drying equipment has been available for more than 20 years [35] for small samples, and large scale equipment construction has been planned. The main difficulty with the technique resides in the safety considerations because of the very high ($\approx$ 72 Atm) pressures required to take the samples to the critical point.

C. Dry Etching:

A number of schemes have been proposed which are based on dry etching of the sacrificial layer. This operation is often difficult if the sacrificial layer is silicon based (such as silicon dioxide) because it requires strong etchants that do not have good selectivities with respect to the suspended element material. Vapor-phase HF etching [40] at elevated temperatures [41, 42] has been often used for this purpose with a high rate of attack of silicon nitride films. The structure can also be easily released by plasma etching if the sacrificial layer is silicon [43].

A more successful series of techniques are based upon the replacement of the sacrificial layer with a weaker solid that can be later removed by a harmless dry etching. These schemes involve primarily the replacement of sacrificial layers with plastics that can be then be etched using O_2 plasma or ozone which are harmless to silicon-based materials. Techniques based upon the use of p-xylylene supports (Figure 13-14) [44] have been successful in releasing polysilicon plates that as large as $3000 \times 3000 \times 1$ μm^3. A technique that is based upon the replacement of the

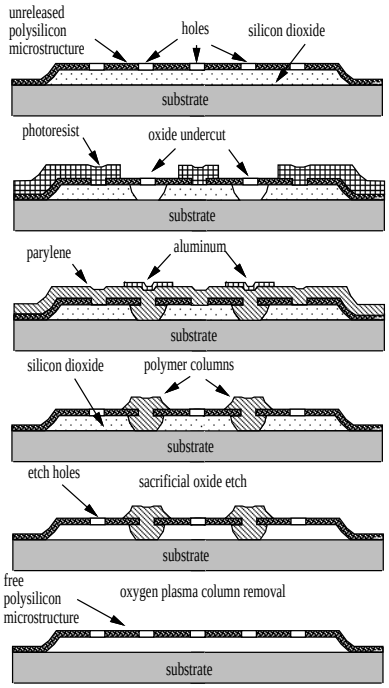

Fig. 13. Construction of polymer support feet that can be dry etched thus releasing the sample.

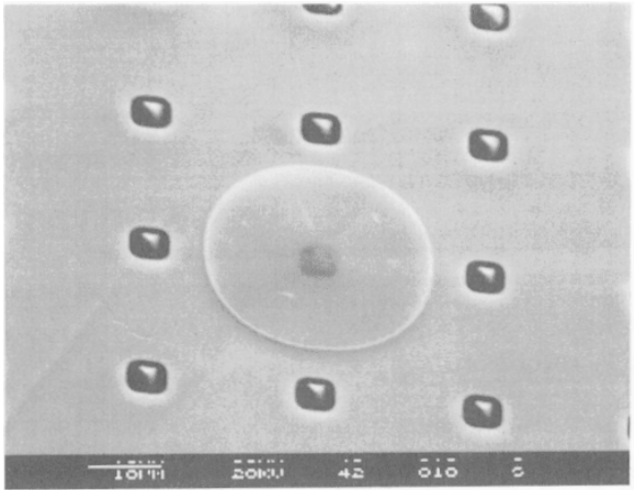

Fig. 14. SEM of underside of sacrificial p-xylylene supports. The plastic supports are etched using oxygen plasma.

rinse solution with resist through a series of dilutions was developed by Orpana and Korhonen [10]. Other techniques include the replacement of the rinse solution with monomers that polymerize in a short time as well as plasma-polymerized fluorinated plastics [45, 46].

D. Liquid Bridge Cleavage:

The strong capillary pull causes the microstructure collapse because as the rinse solution is removed, the liquid volume concentrates near the weakest central part of the suspended member. The impact of the capillary pull may thus be reduced if the liquid droplet is concentrated near the anchors instead. Recently, Abe *et al.* [47] exploited this idea in a very ingenious way. The technique makes use of a sharp corner patterned near the weakest point in the structure. As the liquid is removed, this corner breaks the liquid bridge into two separate droplets that tend to reside near the suspended structure anchors, where the impact of the capillary pull is minimal. Using these idea, very long double-supported beams can be freely released without the need of the techniques described above.

E. Hydrophobic Coatings:

The capillary pull can become a push if the contact angle is made larger than 90 °. The contact angle of aqueous solutions on SiO_2 and Si surfaces was studied by several researchers [48–51]. Oxidized surfaces are hydrophilic with contact angles ranging from $0 - 39°$ depending on the type of oxide and surface treatment. Bare silicon surfaces obtained by the removal of native oxide using HF are hydrophobic. The hydrophobicity has been attributed to possible hydrogen groups [52] attached to the silicon. Contact angles [48] as high as 78° have been reported; however, the native oxide is known to regrow in both water and when exposed to air [53, 54]; thus complete hydrophobicity is difficult to achieve. In order to accomplish a higher contact angle, a chemical change in the surface of the suspended member is required. Recently, a number of well-known [55] hydrophobic self-assembled monolayers (SAM) have been grown on silicon surfaces with successful results [14, 56]. These layers are based on the silanization of silicon surfaces with organic groups by treating the surface with octadecyltrichlorosilane (OTS) precursor molecule ($C_{18}H_{37}SiCl_3$). The procedure first involves the replacement of the aqueous rinse with an organic solvent though a series of dilution steps. The SAM is next grown, and then the solvent is replaced by water through the reverse series of dilutions. Because the silanized surfaces have a very high contact angle ($\approx 114°$), at this stage the water recedes from the surfaces resulting in a sample that emerges dry from the rinse. Cantilever beams at least as long as 1000 μm long were successfully released using this technique with beams as long as 400 μm passing the "in-use" stiction contact test (Figure 15).

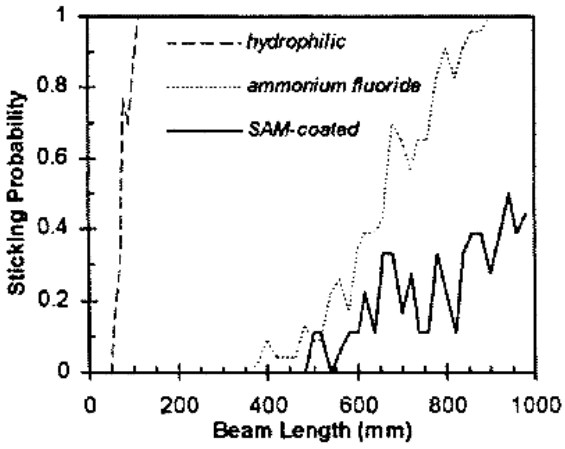

Fig. 15. Sticking probability for cantilever beams that were given different treatments.

It may be possible to eliminate the complex series of dilutions if the hydrophobic film is formed directly in the aqueous

solution. Autophobic films [57, 58] can be grown in silicon dioxide substrates which are immersed in aqueous solutions in the presence of a surfactant. These films can be formed when weakly polar molecules like octadecylamine ($C_{18}H_{37}NH_3$) are dissolved in water. These molecules attach to the solid surface leaving the long hydrophobic tail pointing toward the solution. These type of surfactants are commonly used for the separation of mineral powders by flotation techniques [59, 60].

F. External Release Force:

This technique uses an external force to free a pinned suspended member. Samples which are pinned to the substrate can often be freed by the application of a small shear force (often by using a probe tip). A practical implementation of this scheme has been developed [61]. The technique involves the construction of a wire on top of the suspended member. An upward force can then be generated during electrical testing by discharging a capacitor through the wire in the presence of a magnetic field as shown in Figure 16. The technique has been successfully applied to the release of beams and plates as shown in Figure 17 with 100% yields with typical discharges of 0.5 μC.

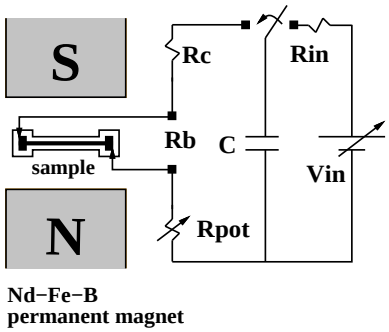

Fig. 16. Release of pinned microstructure by Lorentz force. The suspended member is placed between the poles of a permanent magnet and a capacitor is discharged across it.

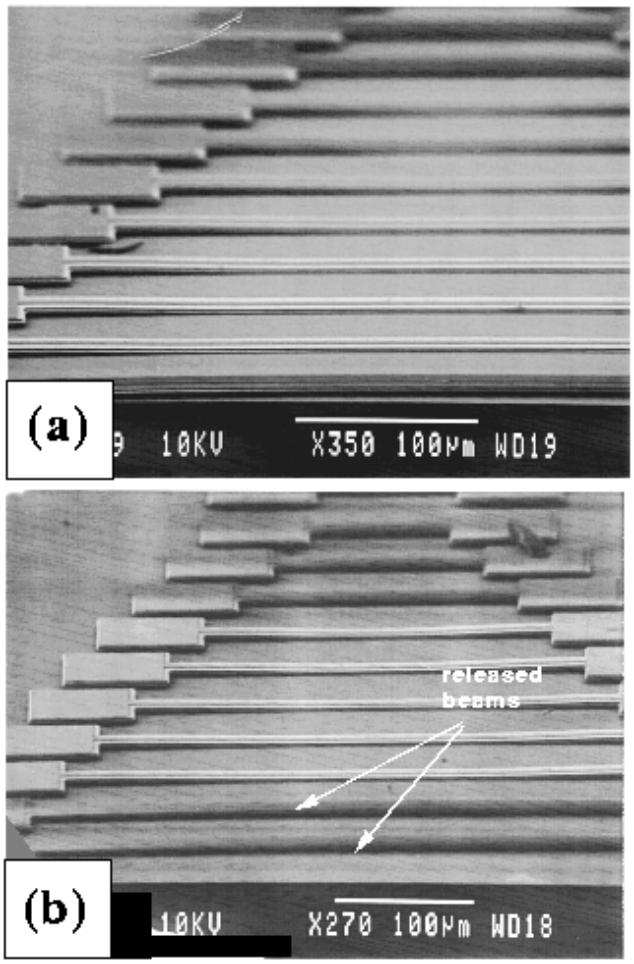

Fig. 17. Array of doubly-supported beams (a) before and (b) after the application of the discharge. The last two beams were released by the Lorentz force.

The main difficulty with the technique resides in the construction of the wire which may cause unnecessary warping of the suspended member. The technique is also useful to electrically determine whether a microstructure is pinned or freed by examination of the wire *IV* curve.

Most of these techniques (with the exception of coatings) can only eliminate the capillary pull or its effects during its fabrication process. After the sample is packaged, if it is exposed to a high-humidity environment or a shock, the pinning may return hence becoming a reliability issue. Therefore these techniques are insufficient to effectively eliminate the adhesion failure but rather delay it. A permanent solution to the problem also requires additional treatments that attempt to reduce the intersolid adhesion. These are discussed below.

V. Reduction of Intersolid Adhesion

A permanent elimination of the adhesion failure requires the reduction of the intersolid surface adhesion. Several techniques have been developed toward this goal. The main ones are listed below.

A. Use of Textured Surfaces and Posts:

The adhesion force can be readily reduced if the contact area between the elastic member and the substrate is reduced. In practice, this can be accomplished by texturing the contact surface. This may be done through the generation of a rough interface [62, 63]. Yee [63] reported an increase in the detachment length of approximately two by the oxidation and dry etching of a polysilicon supporting surface.

The texturing can also be deliberately introduced by constructing a periodic array of small supporting post, commonly known as “dimples”. These supports are constructed by etching small indentations into the sacrificial layer before the deposition of the suspended member as shown in Figure 18 causing the formation of a protrusion in the structural layer (Figure 19). This method was first used by L. S. Fan [64] for the construction of a micromotor, and later applied to comb drives [65]. The force required to detach a semi spherical dimple of radius R is easily shown to be [66, 67]

$$F = (3/2)\,\pi\gamma_s R \tag{20}$$

thus it becomes zero as $R \to 0$. Furthermore, the dimple approach benefits from the fact that in general the suspended member will be supported by only three posts (in much the same

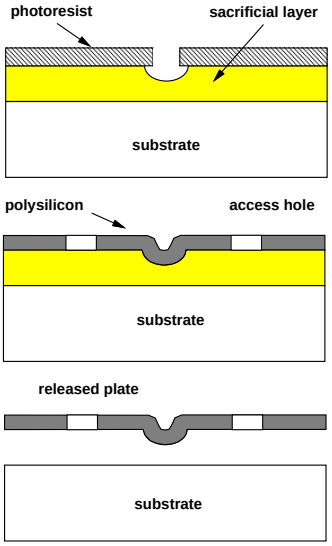

Fig. 18. Construction of dimple posts.

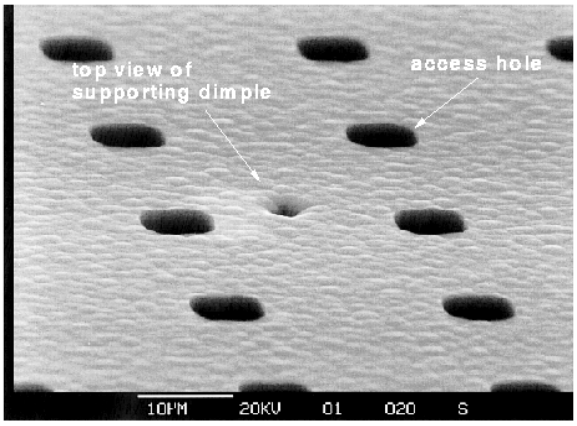

Fig. 19. SEM photograph of a typical dimple on a polysilicon plate.

way that a table with irregular legs is only supported by three of them). This technique is very simple but it suffers from two drawbacks.

First, the dimple method cannot be applied for microstructures with flat surfaces as required in many transducer designs. Second, the adhesion of the dimple is often larger than that anticipated by Eq. (20) when drying out the sample. This is believed to be associated with the formation of an often visible solid bridge of SiO_2 as the water evaporates [53].

B. Low-Energy Monolayer Coatings:

These coatings are the same hydrogenated and OTS-type monolayers discussed above. If their intersolid adhesion energy is sufficiently low, this option is very attractive since it eliminates both failure originating mechanisms. Recently, Houston *et al.* [56] performed contact tests in silicon microstructures with surfaces that were terminated with hydrogen bonds, and coated with OTS self-assembled monolayers. Preliminary tests suggested that cantilever beams as long as 1000 μm-long exhibited about 50 % sticking probability on OTS-coated samples after they are brought in contact with the substrate (Figure 15). These films have been reported to show an extremely low effective adhesion energy ($3\ \mu Jm^{-2}$).

The main difficulty associated with many of these films is their extreme fragility. Because the SAM films are extremely thin (≈2.5 nm), they have a high tendency to degrade at elevated temperatures, as shown in Figure 21. [56]. The aging behavior of hydrogen terminated surfaces has also been observed by Houston *et al.* [68] as shown in Figure 20 indicating that these surfaces chemically react with contaminants over time.

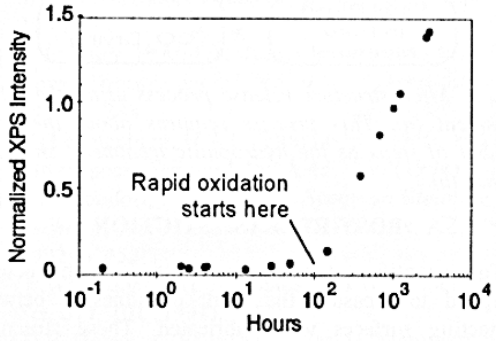

Fig. 20. Degradation of low-energy coating formed by NH_4F treatment. The plot indicates the passivating monolayer degrades after 100 hours of exposure to atmospheric conditions.

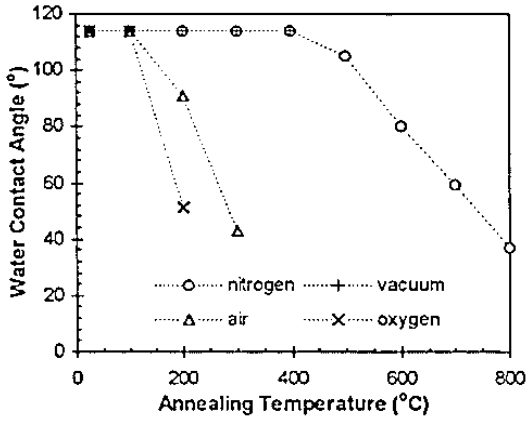

Fig. 21. Degradation of the contact angle in self-assembled OTS coatings exposed 5 minutes to various environments.

These films however remain effective inside sealed, controlled environments at thermal equilibrium where degrading reactions cannot take place, and any vaporization is henceforth followed by a redeposition.

Similar monolayer films are currently used in sealed deformable mirror displays under this strictly controlled environment [69]. This inherent need for a suitable packaging technology has become a driver for the development of micropackages in MEMS devices [70].

C. Fluorinated Coatings:

Fluorinated hydrocarbon coatings consisting of CF_x chains have very low surface energies; hence they are likely candidates coatings for the reduction of intersolid adhesion. TFE-like layers can be grown in many different ways [71]. A common way

to grow these films is by plasma polymerization [72–74]. Often the growth of these films is highly directional with most of the growth occurring in the surfaces exposed to the plasma [46]. In order for these films to be effective, the film must be capable of growth under a covered surface.

Fluorinated films can also be grown at a much reduced rate in zones which are not directly exposed to the plasma [75]. In this regime, the deposition rate is a diffusion-limited process which is not subject to the rapid decay of the plasma density resulting in a much more uniform deposition. This idea has been recently exploited by Man *et al.* [76, 77] to deposit near conformal TFE-like films in silicon microstructures. Using this technique, the deposition takes place inside a Faraday cage that prevents the plasma from reaching the sample as shown in Figure 22. These

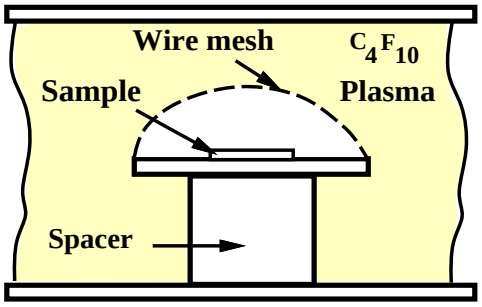

Fig. 22. Setup used for deposition of TFE-like films

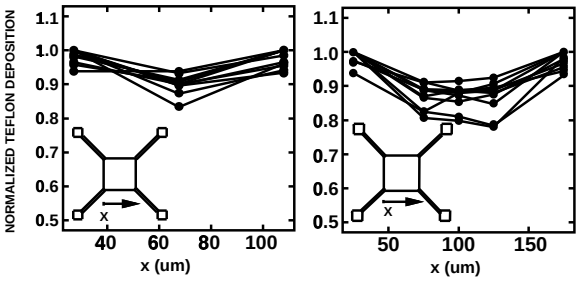

Fig. 23. Uniformity of TFE-like films on the underside of suspended plates. The front of the plate has approximately twice the thickness as the underside.

fluorinated films can be quite thick (> 20 nm) hence durable and have a contact angle of about 108 °.

Periodic wear and temperature tests have been performed in these films as shown in Figure24. The results predict a projected mean time to failure (determined by a loss in the hydrophobicity) greater than 10 years at 150 °C in atmospheric conditions. The films remain hydrophobic even at very high temperatures and display little wear even after 10^7 contact cycles.

Of all the above adhesion prevention methods, the low-energy coatings are the most effective and reliable. The monolayer technique is especially attractive in the sense that it solves both capillary pull and adhesion problems with only one application, but it requires a sealed package to maintain the long term monolayer integrity. Thicker films are more robust and can survive atmospheric conditions for many years but these require the use of a complementary technique to eliminate the capillary pull during the device fabrication. Perhaps the best solution is a combination of both techniques.

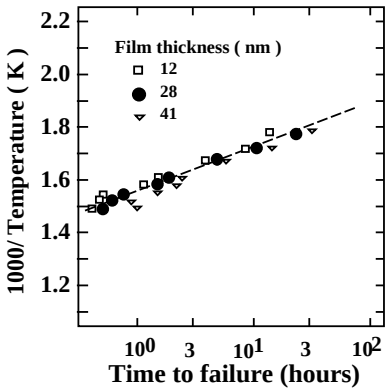

Fig. 24. Degradation of TFE-like plasma polymerized coatings under atmospheric conditions at different temperatures. These films remain on the sample for many years.

The thickness of the film is not only determined by the durability desired but also by how it affects the device structure. In cases where the structure must have high quality factor, a thin layer is desired; while other structures may be more suited to thicker, stronger films.

VI. Summary

This paper reviews the sources causing adhesion-related failures in microelectromechanical systems. These failures are caused by the fact that MEMS devices are extremely susceptible to surface forces because they are very fragile and in very close proximity to their substrates hence causing suspended elastic members to stick to their substrates. The failure originates from the presence of a collapsing force which may be external or originated by capillary forces when the suspended part is exposed to a liquid. this is then followed by a strong intersolid adhesion capable of overcoming the elastic member restoring force. The behavior of the microstructure under these two phenomena has been examined. Several practical techniques for the elimination of the collapsing force and the intersolid adhesion are discussed.

References

[1] K. Chau, C. Fung, P. R. Harris, and G. Dahrooge, "A verstile polysilicon diaphragm pressure sensor chip," in *Int. Electron Devices Meeting, (IEDM 91)*, pp. 695–697, 1991.

[2] D. W. Burns, *Micromechanics of Integrated Sensors and the Planar Processed Pressure Transducer*. PhD thesis, University of Winsconsin, Madison, 1988.

[3] J. M. Lysko, E. Stolarski, and R. S. Jachowicz, "Capacitive silicon pressure sensor based on the one-side wafer processing," in *Transducers' 91*, pp. 685–688, 1991.

[4] J. T. Kung and H.-S. Lee, "An integrated air-gap capacitor process for sensor applications," in *Transducers' 91*, pp. 312–314, 1991.

[5] W. Yun, R. T. Howe, and P. R. Gray, "Surface micromachined, digitally force-balanced accelerometer with integrated CMOS detection circuitry," in *International Workshop on Solid-State Sensors and Actuators (Hilton Head' 92)*, pp. 126–131, 1992.

[6] L. Ristic, R. Gutteridge, B. Dunn, D. Mietus, and P. Bennett, "Surface micromachined polysilicon accelerometer," in *International Workshop on Solid-State Sensors and Actuators (Hilton Head' 92)*, pp. 118–121, 1992.

[7] H. Guckel and D. W. Burns, "Fabrication of micromechanical devices from polysilicon films with smooth surfaces," *Sensors and Actuators*, vol. 20, pp. 117–122, 1989.

[8] H. Guckel, J. J. Sniegoeski, and T. R. Christenson, "Advances in processing techniques for silicon micromechanical devices with smooth sur-

faces," in *International Workshop on Micro Electromechanical Systems (MEMS'89)*, pp. 71–75, 1989.
[9] P. R. Scheeper, J. R. Voorthuyzen, and P. Bergveld, "Surface forces in micromachined structures," in *Micromechanics Europe 1990 (MME '90)*, pp. 26–31, 1990.
[10] M. Orpana and A. O. Korhonen, "Control of residual stress of polysilicon thin films by heavy doping in surface micromachining," in *Transducers' 91*, pp. 957–960, 1991.
[11] N. Takeshima, K. J. Gabriel, M. Ozaki, J. Takashashi, H. Horiguchi, and H. Fujita, "Electrostatic parallelogram actuators," in *Transducers' 91*, pp. 63–66, 1991.
[12] H. C. Nathanson and J. Guldberg, "Topologically structured thin films in semiconductor device operation," *Physics of Thin Films*, vol. 8, pp. 251–298, 1975.
[13] A. D. Zimon, *Adhesion of Dust and Powder*. New York: Consultants Bureau, 1982.
[14] R. Alley, R. T. Howe, and K. Komvopoulos, "The effect of release-etch processing on surface microstructure stiction," in *International Workshop on Solid-State Sensors and Actuators (Hilton Head' 92)*, pp. 202–207, 1992.
[15] J. N. Israelachvili, *Intermolecular and Surface Forces*. New York: Academic Press, 1985.
[16] C. H. Mastrangelo and C. H. Hsu, "Mechanical stability and adhesion of microstructures under capillary forces– parts I and II," *Journal of Microelectromechanical Systems*, vol. 2, pp. 33–55, 1993.
[17] M. A. Fortes, "Axisymmetric liquid bridges between parallel plates," *J. Colloid and Interface Science*, vol. 88, pp. 338–352, 1982.
[18] W. C. Carter, "The forces and behavior of fluids constrained by solids," *Acta Metallurgica*, vol. 36, pp. 2283–2292, 1988.
[19] R. Finn, *Equilibrium Capillary Surfaces.* New York: Springer-Verlag, 1986.
[20] J. F. Padday, A. R. Pitt, and R. M. Pashley, "Menisci at a free liquid surface: surface tension from the maximum pull on a rod," *J. Chem. Soc. Faraday Trans. 1*, vol. 10, pp. 1919–1931, 1974.
[21] E. Matijevic, *Surface and Colloid Science*, vol. 2. New York: Wiley, 1969.
[22] V. I. Arnold, *Catastrophe Theory*. New York: Springer-Verlag, 1986.
[23] P. T. Saunders, *An Introduction to Catastrophe Theory*. Cambridge: Cambridge University Press, 1990.
[24] T. Poston and I. Stewart, *Catastrophe Theory and its Applications.* London: Pitman, 1978.
[25] M. S. El Naschie, *Stress. Stability, and Chaos in Structural Engineering: An Energy Approach*. New York: McGraw-Hill, 1990.
[26] K. Kendall, "The adhesion and surface energy of elastic solids," *J. Phys. D: Appl. Phys.*, vol. 4, pp. 1186–1195, 1971.
[27] W. P. Maszara, G. Goetz, and J. B. McKitterick, "Bonding of silicon wafers for silicon-on-insulator," *J. Appl. Phys*, vol. 64(10), pp. 4943–4950, 1988.
[28] P. P. Gillis and J. J. Gilman, "Double-cantilever cleavage mode of crack propagation," *J. Appl. Phys*, vol. 35(3), pp. 647–658, 1964.
[29] J. J. Gilman, "Direct measurements of the surface energies of crystals," *J. Appl. Phys*, vol. 31(12), pp. 2208–2218, 1960.
[30] R. L. Mullen, N. Mehrengany, M. P. Omar, and W. H. Ko, "Theoretical modeling of boundary conditions in microfabricated beams," in *International Workshop on Micro Electromechanical Systems (MEMS'91)*, pp. 154–159, 1991.
[31] Q. Meng, M. Mehregany, and R. L. Mullen, "Theoretical modeling of microfabricated beams with elastically restrained supports," *IEEE J. Microelectromechanical Sys.*, pp. 128–137, 1993.
[32] C. H. Mastrangelo and C. H. Hsu, "A simple experimental technique for the measurement of the work of adhesion of microstructures," in *International Workshop on Solid-State Sensors and Actuators (Hilton Head' 92)*, pp. 208–212, 1992.
[33] M. Harmening, W. Bacher, P. Bley, A. El-Kholi, H. Kalb, B. Kowanz, W. Menz, A. Michel, and J. Mohr, "Molding of three-dimensional microstructures by the LIGA process," *Proc. IEEE Micro Electro Mech. Syst. Workshop*, Travemünde, Germany, Feb. 1992, pp. 202–207.
[34] A. B. Frazier and M. G. Allen, "High aspect ratio relectroplated microstructures using a photosensitive polyimide process," *Proc. IEEE Micro Electro Mech. Syst. Workshop*, Travemünde, Germany, Feb. 1992, pp. 87–92.
[35] C. J. Dawes, *Introduction to Biological Electron Microscopy: Theory and Techniques.* Burlington, VT: Ladd Research Industries, 1988.
[36] E. W. Flosdorf, *Freeze Drying: Drying by Sublimation.* Ann Arbor, MI: University Microfilms International, 1982.
[37] R. O. Holler, *Freeze-Drying Biological Specimens.* Washington, DC: Smithsonian Institution Press, 1979.
[38] J. D. Mellor, *Fundamentals of Freeze Drying*. New York: Academic Press, 1978.
[39] G. T. Mulhern, D. Soane, and R. T. Howe, "Supercritical carbon dioxide drying for microstructures," in *Transducers' 93*, pp. 296–299, 1993.
[40] H. Watanabe, S. Ohnishi, I. Honma, H. Kitajima, H. Ono, R. WIlhelm, and A. Sophie, "Selective etching of phosphosilicate glass with low pressure vapor hf," *J. Electrochem. Soc.*, vol. 142, pp. 237–243, 1995.
[41] M. Wong, M. Moslehi, and R. Bowling, "Wafer temperature dependence of the vapor-phase hf oxide etch," *J. Electrochem. Soc.*, vol. 140, pp. 205–208, 1993.
[42] J. Ruzillo, K. Torek, C. Daffron, R. Grant, and R. Novak, "Etching of thermal oxides in low pressure anhydrous HF/CH_3OH gas mixture at elevated temperature," *J. Electrochem. Soc.*, vol. 140, pp. p. L64–L66, 1993.
[43] T. Hirano, T. Furuhata, and H. Fujita, "Dry releasing of electroplated rotational and overhanging structures," in *International Conference on Micro Electromechanical Systems (MEMS 93)*, Fort Lauderdale, FL, U.S.A. Feb. 1993, pp. 278–283.
[44] C. Mastrangelo and G. Saloka, "A dry-release method based on polymer columns for microstructure fabrication," *Proc. IEEE Micro Electro Mech. Syst. Workshop*, Fort Lauderdale, FL, U.S.A. Feb. 1993, pp. 77–81.
[45] F. Kozlowski, N. Lindmair, T. Scheiter, C. Hierold, and W. Lang, "A novel method to avoid sticking of surface micromachined structures," *Transducers'95*, pp. 220–223, 1995.
[46] H. V. Jansen, J. G. E. Gardeniers, J. Elders, H. A. C. Tilmans, and M. Elwenspoek, "Applications of fluorocarbon polymers in micromechanics and micromachining," *Sensors and Actuators*, vol. A41-42, pp. 136–140, 1994.
[47] T. Abe, W. C. Messner, and M. Reed, "Effective methods to prevent stiction during post-release-etch processing," *Proc. IEEE Micro Electro Mech. Syst. Workshop*, Amsterdam, Neth, Feb. 1995, pp. 94–99.
[48] G. Gould and E. A. Irene, "An in-situ study of aqueous HF treatment of silicon by contact angle measurement and ellipsometry," *J. Electrochem. Soc.*, vol. 135, pp. 1535–1539, 1988.
[49] R. Williams and A. M. Goodman, "Wetting of thin layers of SiO_2 by water," *Applied Physics Letters*, vol. 25, pp. 531–532, 1974.
[50] R. G. Frieser, "Characterization of thermally grown SiO_2 surfaces by contact angle measurements," *J. Electrochem. Soc.*, vol. 121, pp. 669–672, 1974.
[51] K. Hermansson, U. Lindberg, B. Hök, and G. Palmskog, "Wetting properties of silicon surfaces," in *Transducers' 91*, pp. 193–196, 1991.
[52] D. Graf, M. Grunder, R. Schulz, and L. Muhlhoff, "Oxidation of hf-treated si wafer surfaces in air," *J. Applied Phys.*, vol. 68, pp. 5155–5161, 1990.
[53] H. Watanabe, M. Hamano, and M. Harazono, "The role of atmospheric oxygen and water in the generation of water marks on the silicon surface in cleaning processes," *Mat. Sci. Eng.*, vol. B4, pp. 401–405, 1989.
[54] M. Morita, T. Ohmi, E. Hagesawa, M. Kawakami, and K. Suma, "Control factor of native oxide growth on silicon in air or in ultrapure water," *Applied Physics Letters*, vol. 55, pp. 562–564, 1989.
[55] A. Ulman, *An Introduction to Ultrathin Organic Films: From Langmuir-Blodgett to Self-Assembly*. Boston: Academic Press, 1991.
[56] M. Houston, R. Maboudian, and R. T. Howe, "Self-assembled monolayer films as durable anti-stiction coatings for polysilicon microstructures," in *International Workshop on Solid-State Sensors and Actuators (Hilton Head' 96)*, pp. 42–47, 1996.
[57] E. G. Shafrin and W. A. Zisman, "Hydrophobic monolayers adsorbed from aqueous solution," *J. Colloid Science*, vol. 4, pp. 571–589, 1949.
[58] E. G. Shaffrin and W. A. Zisman, "Hydrophobic monolayers and their adsorption from aqueous solution," in *Monomolecular Layers* (H. Sobotka, ed.), pp. 129–160, American Association for the Advancement of Science, 1954.
[59] K. L. Sutherland and I. W. Wark, *Principles of Flotation.* Melbourne: Australasion Institute of Mining and Metallurgy, 1955.
[60] L. Holland, *The Properties of Glass Surfaces*. New York: Wiley, 1964.
[61] B. P. Gogoi and C. H. Mastrangelo, "Adhesion release and yield enhancement of microstructures using pulsed lorentz forces," *Journal of Microelectromechanical Systems*, vol. 4, pp. 185–192, 1995.
[62] R. L. Alley, P. Mai, K. Komvopulos, and R. T. Howe, "Surface roughness modification of interfacial contacts in polysilicon microstructures," in *Transducers' 93*, pp. 288–291, 1993.
[63] Y. Yee, K. Chun, and J. D. Lee, "Polysilicon surface modification technique to reduce sticking of microstructures," in *Transducers' 95*, pp. 206–209, 1995.
[64] L.-S. Fan, *Integrated Micromachinery – Moving Structures in Silicon Chips*. PhD thesis, University of California, Berkeley, 1990.
[65] W. C. Tang, T.-C. H. Nguyen, and R. T. Howe, "Laterally driven polysilicon resonant microstructures," *Proc. IEEE Micro Electro Mech. Syst. Workshop*, Salt Lake City, Utah, U.S.A., Feb. 1989, pp. 53–59.
[66] K. L. Johnson, K. Kendall, and A. D. Roberts, "Surface energy and the contact of elastic solids," *Proc. Royal Soc. London A*, vol. 324, pp. 301–313, 1971.

[67] K. L. Johnson, *Contact Mechanics*. New York: Cambridge University Press, 1987.
[68] M. R. Houston, R. Maboudian, and R. T. Howe, "Ammonium fluoride anti-stiction treatments for polysilicon microstructures," *Transducers'95*, pp. 210–213, 1995.
[69] L. J. Hornbeck, "Digital light processing and MEMS: timely convergence for a bright future," in *Proc. SPIE Micromachining and Microfabrication Process Technology Conference*, vol. SPIE 2639, pp. 1–21, 1995.
[70] M. B. Cohn, Y. Liang, R. T. Howe, and A. P. Pisano, "Wafer-to-wafer transfer of microstructures for vacuum packaging," in *International Workshop on Solid-State Sensors and Actuators (Hilton Head' 96)*, pp. 32–35, 1996.
[71] J. J. Licari, *Plastic Coatings for Electronics*. New York: McGraw-Hill, 1970.
[72] H. Yasuda and T. Hsu, "Some aspects of plasma polymerization of fluorine containing organic compounds," *J. Polym. Sci. Polym Chem. Ed.*, vol. 15, pp. 2411–2424, 1977.
[73] H. Yasuda and T. Hsu, "Some aspects of plasma polymerization of fluorine containing organic compounds. ii. comparison of ethylene and tetrafluoroethylene," *J. Polymer Sci.*, vol. 16, pp. 415–425, 1978.
[74] H. Yasuda, *Plasma Polymerization*. New York: Academic Press, 1985.
[75] P. D. Buzzard, *Plasma Polymerization of Tetrafluoroethylene in a Field Free Zone*. PhD thesis, University of California, Berkeley, 1978.
[76] P. F. Man, B. P. Gogoi, and C. H. Mastrangelo, "Elimination of post-release adhesion in microstructures using thin conformal fluorocarbon films," *Proc. IEEE Micro Electro Mech. Syst. Workshop*, San Diego, CA, U.S.A. Feb. 1996, pp. 55–60.
[77] P. F. Man, B. P. Gogoi, and C. H. Mastrangelo, "Elimination of post-release adhesion in microstructures using conformal fluorocarbon films," *Journal of Microelectromechanical Systems*, vol. 5, March 1997.